Deep South Atlantic carbonate chemistry and increased interocean deep water exchange during last deglaciation

Jimin Yu[1,2*], Robert F. Anderson[3*], Zhangdong Jin[4], Laurie Menviel[5,6], Fei Zhang[4], Fredrick J. Ryerson[2], Eelco J. Rohling[1,7]

[1]*Research School of Earth Sciences, The Australian National University, Canberra, ACT 0200, Australia*
[2]*Lawrence Livermore National Laboratory, 7000 East Av., Livermore, CA, 94550, USA*
[3]*Lamont-Doherty Earth Observatory of Columbia University, 61 Route 9W/PO Box 1000, Palisades, NY, 10964-8000, USA.*
[4]*State Key Laboratory of Loess and Quaternary Geology, Institute of Earth Environment, Chinese Academy of Sciences, Xi'an 710075, China*
[5]*Climate Change Research Centre, University of New South Wales, Sydney, Australia*
[6]*ARC Centre of Excellence for Climate System*
[7]*Ocean and Earth Science, University of Southampton, National Oceanography Centre, Southampton SO14 3ZH, UK*

*Correspondence to: jimin.yu@anu.edu.au (J.Y), boba@ldeo.columbia.edu (R.F.A)

Submit to *Quaternary Science Reviews* as an Article

Highlights:

- New high-resolution [CO_3^{2-}] for the deep S Atlantic during 0-28 kyr;
- Similar deep water [CO_3^{2-}] between late Holocene and LGM;
- Deep water [CO_3^{2-}] decreased, while $\delta^{13}C$ rose during HS1;
- Interocean carbon exchange enhanced during HS1;
- Large [CO_3^{2-}] decline occurred since 10 kyr.

Abstract

Carbon release from the deep ocean at glacial terminations is a critical component of past climate change, but the underlying mechanisms remain poorly understood. We present a 28,000-year high-resolution record of carbonate ion concentration, a key parameter of the global carbon cycle, at 5-km water depth in the South Atlantic. We observe similar carbonate ion concentrations between the Last Glacial Maximum and the late Holocene, despite elevated concentrations in the glacial surface ocean. This strongly supports the importance of respiratory carbon accumulation in a stratified deep ocean for atmospheric CO_2 reduction during the last ice age. After ~9 μmol/kg decline during Heinrich Stadial 1, deep South Atlantic carbonate ion concentration rose by ~24 μmol/kg from the onset of Bølling to Pre-boreal, likely caused by strengthening North Atlantic Deep Water formation (Bølling) or increased ventilation in the Southern Ocean (Younger Drays) or both (Pre-boreal). The ~15 μmol/kg decline in deep water carbonate ion since ~10 kyr is consistent with extraction of alkalinity from seawater by deep-sea $CaCO_3$ compensation and coral reef growth on continental shelves during the Holocene.

Between 16,600 and 15,000 years ago, deep South Atlantic carbonate ion values converged with those at 3.4-km water depth in the western equatorial Pacific, as did carbon isotope and radiocarbon values. These observations suggest a period of enhanced lateral exchange of carbon between the deep South Atlantic and Pacific Oceans, probably due to an increased transfer of momentum from southern westerlies to the Southern Ocean. By spreading carbon-rich deep Pacific waters around Antarctica for upwelling, invigorated interocean deep water exchange would lead to

more efficient CO_2 degassing from the Southern Ocean, and thus to an atmospheric CO_2 rise, during the early deglaciation.

Keywords: deep-sea, carbonate ion, interocean exchange, atmospheric CO_2

1. Introduction

Ice core records reveal stepwise rises in atmospheric CO_2 content since the Last Glacial Maximum (LGM; 22-18 kyr) (Monnin et al., 2001), but the reasons for these changes remain elusive. The large carbon reservoir of the deep ocean is thought to have played an important role in modulating past atmospheric CO_2 changes (Broecker, 1982). A leading hypothesis for the deglacial atmospheric CO_2 rise involves a breakdown of the deep vertical density stratification in the Southern Ocean (Anderson et al., 2009; Burke and Robinson, 2012; Sigman et al., 2010a) that governs the rate of CO_2 exchange between the deep ocean and the atmosphere, a process commonly referred to as "ventilation". The history of deep water carbonate chemistry in the Southern Ocean is critical to inform us about the processes involved in the release of CO_2 to the atmosphere in the past.

Deep water carbonate ion concentration, $[CO_3^{2-}]$, is an important parameter in deciphering the deglacial carbon cycle changes. To a first approximation, $[CO_3^{2-}] \approx$ ALK – DIC, where ALK is alkalinity and DIC is dissolved inorganic carbon, each of which influences the carbon storage in the ocean (Sigman and Boyle, 2000; Sigman et al., 2010a). Thus, a $[CO_3^{2-}]$ record for a key location such as the deep Southern Ocean

would yield critical insights into the processes responsible for past atmospheric CO_2 variations. Until now, a quantitative deep water [CO_3^{2-}] record that can sufficiently resolve millennial timescale variability is lacking in the Southern Ocean. For example, a recently published deep water [CO_3^{2-}] record from the Weddell Sea has only four data points during the last 30,000 years (Rickaby et al., 2010), limiting the use of these results to constrain the processes that have regulated the deglacial rise in atmospheric CO_2. Here, we present the first high-resolution quantitative deep water [CO_3^{2-}] record for the Southern Ocean spanning the last 28,000 years to constrain processes that controlled atmospheric CO_2 variations in the past.

2. Samples and methods

Our reconstruction is based on measurements for sediment core TNO57-21 (41.1°S, 7.8°E, 4,981 m) from the southern Cape Basin, South Atlantic Ocean (Fig. 1). The age model of the core is based on 3 new and 20 published radiocarbon dates (Fig. 2; Table S1) (Barker et al., 2009; Barker et al., 2010). It is impossible to use a single planktonic species for radiocarbon dating due to significant shell fragmentation at depths 0-80 cm (corresponding to ~4-9 kyr) in TNO57-21 and the large sample size requirement for ^{14}C analysis. We thus used mixed planktonic species for our radiocarbon measurements. Radiocarbon dates are calibrated assuming a constant surface reservoir age of 600 years (Barker et al., 2009) using Calib 6.01 (Stuiver and Reimer, 1993) and the Marine 09 curve (Reimer et al., 2009). Using variable surface reservoir ages (Skinner et al., 2010) has negligible influence on our conclusion (Fig. S1). The average sedimentation rate is 15.6 cm kyr^{-1}, which minimizes any influence from bioturbation and facilitates the development of climate records with excellent

temporal resolution. The core site is bathed in Lower Circumpolar Deep Water (LCDW), which fills a large volume of the global deep ocean (Fig. 1). Changes in $[CO_3^{2-}]$ of LCDW thus have far-reaching implications for the global carbon cycle.

Our deep water $[CO_3^{2-}]$ reconstruction is based on 67 B/Ca measurements of the epibenthic (a habitat above the sediment-water interface) foraminiferal species *Cibicidoides wuellerstorfi* (Table S2). About 10 cc wet sediments for each sample (1 cm depth interval) from core TNO57-21 were disaggregated in de-ionized water and wet sieved through 63 μm sieves. All *C. wuellerstorfi*, ranging from ~15 to 30 shells in each sample, were picked for all samples from the 250-500 μm size fraction. The shells were then double checked under a microscope before crushing with due attention to use shells of most consistent morphology for B/Ca analyses throughout the core, to minimize any potential influence from changes in shell morphology (Rae et al., 2011). In general, the starting material for each sample has ~12 to 25 shells, equivalent to ~300 to 600 μg. The shells were cleaned by the "Mg-cleaning" method (Barker et al., 2003; Yu et al., 2007) and B/Ca was measured on ICP-MS using the established procedure (Yu et al., 2005). Foraminiferal B/Ca shows no correlation with Mn/Ca ($R^2 = 0.01$, $P = 0.55$) or Al/Ca ($R^2 = 0.00$, $P = 0.89$) or Fe/Ca ($R^2 = 0.00$, $P = 0.97$) (Fig. S2), indicating that B/Ca is not biased by contamination from diagenetic coatings or silicates.

C. wuellerstorfi B/Ca ratios were converted to seawater $[CO_3^{2-}]$ using a sensitivity of 1.14 μmol/mol per μmol/kg specific to this species, as obtained from a global core-top calibration (Yu and Elderfield, 2007) by: $[CO_3^{2-}]_{downcore} = [CO_3^{2-}$

131 $]_{preindustrial}$ + Δ(B/Ca)/1.14, where the preindustrial $[CO_3^{2-}]$, $[CO_3^{2-}]_{preindustrial}$, is
132 estimated using the GLODAP dataset (Key et al., 2004), and Δ(B/Ca) is the deviation
133 of B/Ca of down-core samples relative to the core-top value. The B/Ca-$[CO_3^{2-}]$ proxy
134 is empirical and the mechanism for the observed relationship remains largely
135 unknown. However, subsequent core-top (Brown et al., 2011; Rae et al., 2011;
136 Raitzsch et al., 2011; Yu et al., 2013a) and down-core (Raitzsch et al., 2011; Yu et al.,
137 2013a; Yu et al., 2010b) studies have strongly corroborated the faithfulness of the
138 B/Ca proxy for deep water $[CO_3^{2-}]$.

139

140 Based on core-top samples, Yu and Elderfield (2007) gave an uncertainty of
141 ~±9 μmol/kg (2σ) in deep water $[CO_3^{2-}]$ for reconstructions using *C. wuellerstorfi*
142 B/Ca. This uncertainty should be treated as the worst scenario error because the
143 calculation included errors associated with hydrographic data (at ~±5-10 μmol/kg in
144 seawater $\Delta[CO_3^{2-}]$) (Key et al., 2004), bioturbation (associated with sedimentation
145 rates), shell morphology influences, inter- and intra-shell variability, and analytical
146 error in B/Ca, all of which have been discussed in Yu et al. (2013a). Reconstruction
147 error in down-core records may be estimated using the variance in B/Ca of duplicate
148 measurements and the sensitivity of B/Ca to $[CO_3^{2-}]$. Down-core reconstruction
149 precision may differ between cores due to different degrees of bioturbation, and could
150 be improved by employing recommendations given in Yu et al. (2013a), which were
151 followed in this study. For example, the reconstruction error is given at ~7 μmol/kg
152 (2σ) in core VM28-122 (Yu et al., 2010b). Unfortunately, it is impossible to make
153 duplicates for TNO57-21 due to the limited quantity of sediment available for this
154 study. Here, we assess the error based on the replicates of a consistency standard

(B/Ca = 150 μmol/mol), which was measured during the course of analyzing samples from core TNO57-21 samples. The average uncertainty (2σ) of this consistency standard is ~±6 μmol/mol in B/Ca, corresponding to an error of ~±5 μmol/kg (2σ) in seawater [CO_3^{2-}] assuming a constant sensitivity of 1.14 μmol/mol per μmol/kg. Compared to VM28-122, the slightly better reconstruction error for core TNO57-21 is expected due to faster sedimentation rates at TNO57-21 (~15.7 cm/kyr at TNO57-21 vs. ~7 cm/kyr at VM28-122), which would minimize bioturbation effects and thus be conducive for improved reconstructions at TNO57-21.

We also measured U-Th isotopes for 36 sediment samples from TNO57-21 to supplement published data (Sachs and Anderson, 2003) and increase the resolution of $CaCO_3$ and alkenone fluxes and of authigenic uranium during last 28,000 years (Fig. 2; Table S3). Uranium and thorium isotopes were measured in aliquots of the 1-cm thick sediment samples from core TN057-21. Measurements were made by isotope dilution ICP-MS. A 0.5-g aliquot of dried sediment was dissolved using mixed acids in the presence of ^{229}Th and ^{236}U spikes. After weighing the final solution, an aliquot (~1.0% by weight) was removed, spiked with ^{230}Th and additional ^{236}U, and diluted with 1% HNO3 + 1% HF. This solution was analyzed without further processing by ICP-MS to measure concentrations of ^{238}U and ^{232}Th. Uranium and Th in the remainder (99%) of the initial solution were purified by anion exchange chromatography, after which ^{234}U, ^{235}U and ^{230}Th were measured by ICP-MS. Details of the method are presented in the work of Fleisher and Anderson (2003). Calculations of $CaCO_3$ and alkenone fluxes and authigenic uranium are given in Sachs and Anderson (2003).

3. Dissolution effect on benthic B/Ca

In the deep ocean, changes in deep water [CO_3^{2-}] (deep water property) and dissolution of carbonate on the sea floor (including deep and pore water dissolution) are often coupled: when deep water [CO_3^{2-}] is low, dissolution tends to increase and vice versa. This sometimes makes it difficult to distinguish whether a decline in benthic B/Ca is due to a decrease in deep water [CO_3^{2-}] or enhanced dissolution. However, strong evidence exists to argue against dissolution as the driver for changes in benthic B/Ca. First, benthic foraminiferal shells are calcified in corrosive deep waters and, when compared with planktonic shells, are more resistant to dissolution on the sea floor (Howard and Prell, 1994). Second, Rose Bengal stained (recently alive) and non-Rose Bengal stained (already dead and exposed to deep waters for a certain amount time) shells from the same core-top samples yield similar B/Ca ratios, suggesting that dissolution does not significantly affect B/Ca (Yu and Elderfield, 2007). Third, the sensitivity of B/Ca to deep water Δ[CO_3^{2-}] is sustained at high [CO_3^{2-}] ranges well above the saturation horizon where dissolution of carbonate is minimal (Raitzsch et al., 2011; Yu et al., 2013a; Yu and Elderfield, 2007), supporting that changes in B/Ca are driven by changes in deep water [CO_3^{2-}], not by dissolution.

An insignificant dissolution effect on benthic B/Ca is further supported by comparisons of B/Ca with dissolution proxies at core TNO57-21 (Fig. S3, S4). Overall, benthic B/Ca display weak correlations ($r^2 < 0.10$, $P > 0.005$; Fig. S4) with the >63 μm size fraction, foraminifera shell fragmentation (>150 μm), and the whole shell number (>150 μm), with the exception of %$CaCO_3$ in which case a significant

correlation is observed (see below). Careful scrutiny of the data reveals that benthic B/Ca and dissolution proxies have varied differently on millennial timescales. For example, benthic B/Ca decreased and increased by ~15 μmol/mol during the transitions into and out of Heinrich Stadial 2 (HS2; 27-24 kyr), respectively, which is not observed in any of the dissolution proxies (Fig. S3). During the LGM, benthic B/Ca remained roughly stable, in contrast to obvious trends exhibited by dissolution proxies (steady increases in the >63 μm fraction, whole shell number and %$CaCO_3$ and a steady decline in fragmentation) (Fig. S3). At the transition from Bølling/Allerød (B/A; 14.5-12.9 kyr) to Younger Dryas (YD; 12.9-11.8 kyr), benthic B/Ca increased by ~10 μmol/mol, compared to substantial decreases in the >63 μm fraction and whole shell number, an increase in foraminifera shell fragmentation, and roughly stable %$CaCO_3$ (Fig. S3).

4. Reliability of $\delta^{13}C$ and B/Ca in *C. wuellerstorfi* for deep water signals

The fidelity of using epifaunal benthic foraminifera (e.g., *Cibicidoides* spp.) in reconstructions of deep water chemistry in the Southern Ocean is a matter of debate. It has been speculated that the extremely low $\delta^{13}C$ in *C. wuellerstorfi* from the glacial deep Southern Ocean might be caused by their habitat preference in a fluff layer where fluid $\delta^{13}C$ is decreased by degradation of organic matter (the "Mackensen effect") (Mackensen et al., 1993). If true, then respiration of biogenic matter should also increase DIC and decrease [CO_3^{2-}] of the microenvironment, resulting in concomitant decreases in $\delta^{13}C$ and [CO_3^{2-}] (this is also true for increased organic matter respiration in deep water). However, [CO_3^{2-}] (this study) and $\delta^{13}C$ (Ninnemann and Charles, 2002) at TNO57-21 display no correlation over the last 28,000 years and

show opposite trends during Heinrich Stadial 1 (HS1; 17.5-14.5 kyr) (Fig. 2A, C). Furthermore, a recent core-top survey shows that *Cibicidoides* reliably records deep water $\delta^{13}C$ in a wide region (~40-80°S) of the South Atlantic (Mackensen, 2012), and the low glacial benthic $\delta^{13}C$ is highly reproducible at various locations from the Southern Ocean (Ninnemann and Charles, 2002). Based on the above, we interpret $\delta^{13}C$ of benthic foraminifera at site TNO57-21 as a reliable recorder of the $\delta^{13}C$ of DIC of bottom waters. From this we infer that processes other than the simple build-up and release of respiratory CO_2 influenced the $\delta^{13}C$ and $[CO_3^{2-}]$ of Cape Basin bottom waters in the past.

5. Deep water $[CO_3^{2-}]$, $\%CaCO_3$, and ^{230}Th-normalized $CaCO_3$ flux

Over the past 28 kyr, B/Ca-derived deep water $[CO_3^{2-}]$ shows similar large-scale variations to sediment carbonate content ($\%CaCO_3$) and ^{230}Th-normalized $CaCO_3$ flux (Sachs and Anderson, 2003) (Fig. 2). Changes in deep water $[CO_3^{2-}]$ explain 43% of the variance in $\%CaCO_3$ in TNO57-21 (Fig. S4). Although $[CO_3^{2-}]$ differs in detail from $\%CaCO_3$ and $CaCO_3$ flux due to secondary factors (see below), the overall agreement corroborates the notion (Anderson et al., 2008; Farrell and Prell, 1989; Hodell et al., 2001) that $CaCO_3$ dissolution, regulated by deep water $[CO_3^{2-}]$, is a significant driver for $CaCO_3$ abundance in sediments of the deep Cape Basin (Hodell et al., 2001), as well as in the deep Indian and Pacific Oceans (Anderson et al., 2008; Farrell and Prell, 1989; Yu et al., 2013a).

Although they are broadly similar over the last 28,000 years (Fig. 2, S4d), sediment %$CaCO_3$ and deep water [CO_3^{2-}] derived from B/Ca in *C. wuellerstorfi* differ in detail. The differences include: (i) from 27-28 kyr to HS2, deep water [CO_3^{2-}] declined, but %$CaCO_3$ remained low; (ii) %$CaCO_3$ displays a clear rising trend by ~30% during the LGM, in contrast to roughly stable deep water [CO_3^{2-}]; (iii) the increase in %$CaCO_3$ halted, but showed no decline as observed in deep water [CO_3^{2-}], during HS1; and (iv) sediment %$CaCO_3$ remained roughly constant from the B/A to the Pre-Boreal (PB; 11.8-10 kyr), when deep water [CO_3^{2-}] rose by ~12 μmol/kg (Fig. 2A). These differences cannot be attributed to dilution of $CaCO_3$ by detrital sediments because %$CaCO_3$ and ^{230}Th-normalized $CaCO_3$ flux show very similar patterns over the course of the past 28,000 years ($R^2 = 0.95$, n = 60, $P<0.0001$) (Fig. 2B) (Sachs and Anderson, 2003). Dissimilar patterns of alkenone flux and %$CaCO_3$ indicate an insignificant role of pore water dissolution in $CaCO_3$ preservation in core TNO57-21 during the last 28 kyr (Sachs and Anderson, 2003) (see Fig. 2B, S9c; SI text). We attributed observed differences between %$CaCO_3$ and [CO_3^{2-}] to secondary processes affecting carbonate abundance in sediments, in addition to deep water [CO_3^{2-}] changes. We speculate that sediment $CaCO_3$ content and flux at the site of TNO57-21 are further influenced by factors including winnowing and focusing of fine carbonate particles by deep currents (Sachs and Anderson, 2003) and changes in surface productivity (Karlin et al., 1992; Lyle et al., 2000; Sachs and Anderson, 2003). These secondary factors complicate the interpretation of $CaCO_3$ accumulation quantitatively in terms of deep-water [CO_3^{2-}]. By contrast, *C. wuellerstorfi* is an epibenthic species that lives above the deep water-sediment boundary and hence records deep water chemistry (Corliss, 1985; Lutze and Thiel, 1989). Benthic B/Ca methodology is based on extensive core-top calibrations (Rae et al., 2011; Raitzsch et al., 2011; Yu et al.,

2013a; Yu and Elderfield, 2007) and its validity is strongly supported by down core studies (Raitzsch et al., 2011; Yu et al., 2013a; Yu et al., 2008; Yu et al., 2010c). In the text, we focus on B/Ca-derived deep water [CO_3^{2-}] for paleoceanographic interpretations.

6. LGM

Deep water [CO_3^{2-}] at TNO57-21 displays similar values during the LGM (86.9±3.4 μmol/kg, n = 18, 1 standard deviation) and the late Holocene (~83.0 μmol/kg, n = 2, 0-5 kyr) (Fig. 2A). Small changes in [CO_3^{2-}] of <~5 μmol/kg between the Holocene and the LGM are also observed in the deep Indian and Pacific Oceans (Fig. 3; SI text) (Anderson and Archer, 2002; Yu et al., 2013a; Yu et al., 2010a). Assuming equilibrium between the surface ocean and the atmosphere, surface water [CO_3^{2-}] would have been ~60 μmol/kg higher than today (preindustrial) during the LGM (Foster, 2008; Lea et al., 1999; Yu et al., 2013b), when atmospheric CO_2 was ~90 part per million by volume (ppmv) lower (Fig. 4H) (Monnin et al., 2001). Although the spatial distribution of surface water [CO_3^{2-}] in the world ocean during the LGM remains undetermined, it is reasonable to expect that the surface waters which contributed to newly formed deep water would have had a substantially higher preformed [CO_3^{2-}] than today. The observation that LGM deep water [CO_3^{2-}] was similar to the present therefore reveals an increased surface-to-deep [CO_3^{2-}] gradient in the LGM ocean (Fig. 3).

In seawater, remineralization of biogenic matter increases DIC but has little influence on ALK, resulting in a net decrease in $[CO_3^{2-}]$. Therefore, the difference between LGM and modern levels of respiratory CO_2 in the deep sea must have been sufficiently large to titrate the greater preformed $[CO_3^{2-}]$ of LGM surface waters down to levels close to those existing in the modern deep ocean. This inferred increase in respiratory CO_2 in the glacial-age deep water is consistent with lower dissolved O_2 concentrations in the deep Pacific Ocean during the LGM (Bradtmiller et al., 2010; Galbraith et al., 2007; Jaccard and Galbraith, 2012). It is also consistent with inferences of increased stratification in the glacial ocean (Burke and Robinson, 2012; Lund et al., 2011), which, by limiting the ventilation of high-DIC deep waters, would have facilitated the buildup of CO_2 in the deep ocean and contributed to the low atmospheric CO_2 levels of the LGM (Sigman and Boyle, 2000; Sigman et al., 2010a).

7. Deep South Atlantic $[CO_3^{2-}]$ evolution since the last deglacial

After a ~2 μmol/kg drop at the very end of the LGM, $[CO_3^{2-}]$ decreased by ~7 μmol/kg at ~16.6 kyr during HS1 to a minimum of ~77 μmol/kg at 15.6 kyr (Fig. 2A, 4B). This decline in $[CO_3^{2-}]$ is independently supported by an increase in shell fragmentation in the same core (Fig. S3) (Barker et al., 2010). A decrease of similar magnitude in deep water $[CO_3^{2-}]$ at the location of TNO57-21 also occurred during HS 2 (Fig. 2). This may imply a systematic link between Heinrich Stadials and changes in deep South Atlantic $[CO_3^{2-}]$ chemistry, although $[CO_3^{2-}]$ changes during previous Heinrich events are to be reconstructed.

Starting at ~14.6 kyr, deep water [CO_3^{2-}] at TNO57-21 increased by ~12 μmol/kg over ~500 years and stayed at about 91 μmol/kg over the remainder of the B/A (Fig. 4B). This increase in deep water [CO_3^{2-}], together with the concurrent >0.3‰ increase in benthic $\delta^{13}C$ (Fig. 4C) (Ninnemann and Charles, 2002) and ~160‰ rise in $\Delta\Delta^{14}C$ [the offset between benthic and contemporary atmospheric $\Delta^{14}C$ (Reimer et al., 2009)] (Fig. 4D) (Barker et al., 2010), can be explained by rapid ventilation of the deep South Atlantic by high-[CO_3^{2-}] and ^{14}C-enriched North Atlantic Deep Water (NADW) (Fig. 1; 4A) (Barker et al., 2010; McManus et al., 2004). NADW reinvigoration is also thought to have been responsible for improved carbonate preservation and for increases in both benthic $\delta^{13}C$ and $\Delta\Delta^{14}C$ at 3.3-3.6 km water depth in the North Pacific at around 14.6 kyr (Fig. S5) (Galbraith et al., 2007). This suggests widespread ventilation of the global abyss by low-DIC NADW, and a sizable carbon loss from the deep ocean. Paradoxically, owing to an efficient offsetting effect from an increase in the biological pump that enhanced respired DIC at intermediate depths in the Indian and Pacific Oceans (Galbraith et al., 2007; Jaccard and Galbraith, 2012), only a small net quantity of CO_2 was released to the atmosphere (~10 ppmv rise in atmospheric CO_2) at the onset of B/A (Fig. 4H) (Monnin et al., 2001).

During the YD and PB, deep water [CO_3^{2-}] at TNO57-21 increased by a further ~12 μmol/kg to a peak value of ~104 μmol/kg at ~10 kyr (Fig. 4B). Given the weakened export of NADW during the YD (Fig. 4A) (McManus et al., 2004), we attribute the rise in deep water [CO_3^{2-}] at TNO57-21 to enhanced ventilation from the Southern Ocean. The formation of Antarctic Bottom Water could be enhanced

343 associated with warming in Antarctica during the YD (Fig. 4I) (Barbante et al., 2006)
344 as simulated by (Menviel et al., 2011), and with intensified upwelling in the Southern
345 Ocean during the YD and PB as inferred from opal accumulation records (Fig. 4E)
346 (Anderson et al., 2009). Whatever combination of ventilation processes occurred in
347 the Southern Ocean, the associated release of CO_2 from the deep ocean to the
348 atmosphere (SI Text) likely contributed to the initial ~0.2‰ drop in $\delta^{13}CO_2$ and 25
349 ppmv rise in atmospheric CO_2 during the YD (Fig. 4G, H) (Monnin et al., 2001;
350 Schmitt et al., 2012).

351

352 Together with the concurrent >0.2‰ increase in benthic $\delta^{13}C$, the peak deep
353 water [CO_3^{2-}] of ~104 μmol/kg at 10 kyr in TNO57-21 (Fig. 4B, C) suggests that
354 ventilation of the deep Cape Basin was further improved during the PB. At this time,
355 besides sustained ventilation from the Southern Ocean (Fig. 4E) (Anderson et al.,
356 2009), the deep Cape Basin ventilation was also affected by low-DIC and high-[CO_3^{2-}
357] NADW (Fig. 1) as inferred from sediment Pa/Th (Fig. 4A) (McManus et al., 2004).
358 During the PB, atmospheric CO_2 reached a plateau while atmospheric $\delta^{13}CO_2$ rose
359 (Fig. 4G, H) (Monnin et al., 2001; Schmitt et al., 2012). This suggests that the net
360 release of CO_2 from the deep ocean was in balance with net uptake by the terrestrial
361 biosphere (Elsig et al., 2009). Insufficient data exist to assess how and where carbon
362 transfer between the deep-sea and the atmosphere occurred during this period. Based
363 on the coeval deep water [CO_3^{2-}] increase at TNO57-21 and sustained high opal fluxes
364 south of the Antarctic Polar Front (Fig. 4E) (Anderson et al., 2009), we suggest that
365 degassing of CO_2 via intensified upwelling in the Southern Ocean (SI Text) may have

366 played a significant role in supplying the carbon required for forest regrowth during
367 the PB.

368

369 Since 10 kyr, deep water [CO_3^{2-}] at TNO57-21 has plunged by ~15 μmol/kg,
370 while benthic $\delta^{13}C$ in the same core has remained relatively stable (Fig. 4B, C). The
371 stable benthic $\delta^{13}C$, which is sensitive to the accumulation of respiratory CO_2,
372 indicates that the [CO_3^{2-}] decline must have resulted from a greater decrease in
373 oceanic ALK than in oceanic DIC. This inferred ALK decrease is consistent with two
374 contributing factors inferred from modeling studies (Broecker and Peng, 1987;
375 Menviel and Joos, 2012; Opdyke and Walker, 1992; Ridgwell et al., 2003): (*i*) $CaCO_3$
376 compensation and (*ii*) burial of $CaCO_3$ on continental shelves (SI Text). Owing to its
377 high sedimentation rate, our record reveals for the first time a clear acceleration of the
378 [CO_3^{2-}] decline at ~8 kyr (Fig. 4B), when the substantial regrowth of corals on
379 continental shelves occurred (Vecsei and Berger, 2004). Detailed reconstruction of
380 deep water [CO_3^{2-}] changes is critical for evaluating the influence of different factors
381 on Holocene atmospheric CO_2 (Elsig et al., 2009; Menviel and Joos, 2012; Ridgwell
382 et al., 2003). Due to its detailed features and minimal influence from bioturbation at a
383 key location in the Southern Ocean, our record provides exceptional constraints for
384 models to better quantify the relative contributions of various processes to the 20
385 ppmv rise in atmospheric CO_2 since ~8 kyr (Fig. 4H) (Monnin et al., 2001).

386

387 **8. Increased interocean deep water exchange during HS1**

An intriguing feature of our record is the ~7 μmol/kg decline in [CO_3^{2-}] during HS1 (Fig. 4B), which contrasts with contemporary [CO_3^{2-}] increases previously observed in the deep Indian and Pacific Oceans (Yu et al., 2010a). It appears that the [CO_3^{2-}] decline mainly occurred during the late HS1 (14.5-16.6 kyr) (Fig. 4B). Two-phase changes during HS1 have been observed in many, but not all (such as Pa/Th; Fig. 4A), high-resolution marine and ice core records (Broecker and Putnam, 2012). Since our [CO_3^{2-}] record is the first to resolve millennial timescale changes in the deep South Atlantic, it would be premature at this stage to discuss two-phase [CO_3^{2-}] changes within HS1 without more records of equal resolution. We thus treat the [CO_3^{2-}] decline as occurring broadly during HS1, making no attempt to interpret features within HS1. We acknowledge that if the two-phase [CO_3^{2-}] change is confirmed by additional records in the future, then our interpretation may need to be revised.

The [CO_3^{2-}] decline during HS1 is surprising and counterintuitive, given the intensified upwelling in the Southern Ocean suggested by increased opal fluxes (Fig. 4E) (Anderson et al., 2009). Everything else being equal, transfer of CO_2 from the deep ocean to the surface ocean and the atmosphere by upwelling should deplete DIC and hence increase [CO_3^{2-}] in the deep Southern Ocean during HS1, opposite to our reconstruction (Fig. 4B). The decrease in [CO_3^{2-}] at TNO57-21 coincides with ~0.2‰ increase in benthic $\delta^{13}C$ (Fig. 4B, C) (Ninnemann and Charles, 2002), and this combination rules out the possibility that the observed decline in [CO_3^{2-}] during HS1 reflects reduced penetration of high-[CO_3^{2-}] and high-$\delta^{13}C$ NADW relative to low-[CO_3^{2-}] and low-$\delta^{13}C$ LCDW (Fig. 1) (Key et al., 2004; Yu et al., 2010a). We can also

412 dismiss a phytodetritus effect (Mackensen et al., 1993) on benthic $\delta^{13}C$ based on the
413 high reproducibility of $\delta^{13}C$ (Ninnemann and Charles, 2002) and the absence of any
414 correlation between $\delta^{13}C$ and $[CO_3^{2-}]$ at TNO57-21 (Section 4). Any increased
415 organic matter respiration in deep water at the site would decrease both $\delta^{13}C$ and
416 $[CO_3^{2-}]$, which is not observed during HS1. Instead, we propose in the following a
417 new explanation that is consistent with all observations, which invokes increased
418 admixture of a deep Pacific water mass as the cause of the concurrent $\delta^{13}C$ rise and
419 $[CO_3^{2-}]$ drop in the deep Cape Basin.

420

421 Today, deep water $[CO_3^{2-}]$ is lower in the Pacific Ocean than in the deep Cape
422 Basin (Fig. 1). This $[CO_3^{2-}]$ gradient was even greater during the LGM, as illustrated
423 by comparing reconstructed $[CO_3^{2-}]$ records from TNO57-21 and core MW91-9
424 GGC48 (0°, 161°E, 3,400 m) (GGC48 hereafter) from the Western Equatorial Pacific
425 (WEP; Fig. 1, 4B) (Yu et al., 2010a). The two cores also display large contrasts in
426 benthic $\delta^{13}C$ during the LGM, with Pacific values up to ~0.5‰ higher, despite similar
427 Holocene values (Fig. 4C) (Ninnemann and Charles, 2002; Yu et al., 2010a). The
428 lower glacial benthic $\delta^{13}C$ at TNO57-21 does not necessarily imply a greater burden
429 of respired CO_2 at the site, because deep water $\delta^{13}C$ is further influenced by factors
430 such as preformed values and air-sea exchange (Broecker and Maier-Reimer, 1992;
431 McCave et al., 2008). But benthic $\delta^{13}C$ may be used to assess past deep water mixing
432 (Curry and Oppo, 2005), and we find the deep water $\delta^{13}C$ in different sectors of the
433 Southern Ocean and in the equatorial Pacific Ocean displayed much larger contrasts
434 during the LGM, indicating reduced interocean exchange of deep water than today
435 (Fig. 5). In addition, a larger $\Delta\Delta^{14}C$ gradient is observed between core TNO57-21 and

436 WEP core MD01-2386 (1.1°N, 130°E, 2,820 m) during the LGM (Fig. 4D) (Barker et
437 al., 2010; Broecker et al., 2007; Key et al., 2004), further supporting the inferred
438 glacial reduction in the interocean exchange of deep water.

439

440 Overall, therefore, we infer that the LGM ocean was characterized not only by
441 reduced vertical mixing associated with enhanced stratification (Burke and Robinson,
442 2012; Lund et al., 2011), but also by an increased chemical dissimilarity between deep
443 waters in the Atlantic and Pacific Oceans (Fig. 4B-D, 5). This combination supports
444 the view (McCave et al., 2008) that deep water masses in the world's ocean basins
445 were physically more isolated from each other during the LGM due to reduced lateral
446 exchange via the Southern Ocean.

447

448 During the early deglaciation, the deep water [CO_3^{2-}] gradient between
449 TNO57-21 and GGC48 started to diminish, as [CO_3^{2-}] at TNO57-21 fell and [CO_3^{2-}]
450 at GGC48 rose (Fig. 4B) (Yu et al., 2010a). The deep water [CO_3^{2-}] at both sites
451 reached comparable values during late HS1 (~15.8-14.6 kyr), the only time when
452 complete convergence in [CO_3^{2-}] occurred over the last 28,000 years (Fig. 4B).
453 During HS1, benthic $\delta^{13}C$ and $\Delta\Delta^{14}C$ at site TNO57-21 also converged with those at
454 3.4 and 2.8 km water depths in the WEP, respectively (Fig. 4C, D), as well as with
455 those at 3.8 km water depth in the South Atlantic (Skinner et al., 2010) and 2.7-3.6 km
456 water depth in the North Pacific (Galbraith et al., 2007) (Fig. S5, S6).

457

458 A change in each of our examined proxies by itself may be caused by multiple
459 processes. For example, benthic $\delta^{13}C$ is further influenced by factors in addition to
460 interocean exchange of deep water, including gas exchange and preformed water
461 chemistry. Benthic $\Delta\Delta^{14}C$ may be complicated by changes in surface reservoir ages,
462 but this has negligible influence on the HS1 $\Delta\Delta^{14}C$ convergence between deep South
463 Atlantic and Pacific records (Fig. S7). However, an extraordinary coincidence would
464 be required to explain the convergence observed in all three proxies by invoking
465 simultaneous changes in the preformed chemistry of the different water masses.
466 Instead, it is most straightforward to attribute the concurrent convergence of all three
467 proxies to better mixing of deep waters between the South Atlantic and Pacific
468 Oceans during HS1 than during the LGM. Our interpretation is also consistent with a
469 wider suite of geochemical proxies including neodymium isotopes and authigenic
470 uranium from TNO57-21 (Fig. S8, S9; SI text) (Piotrowski et al., 2012; Piotrowski et
471 al., 2005; Sachs and Anderson, 2003). It is worth noting that increased interocean
472 deep water exchange during HS1 differs from ventilation of global abyssal ocean at
473 the onset of B/A (see above), when the formation of low-DIC NADW was much
474 strengthened compared to HS1 (Fig. 4A) (McManus et al., 2004).

475

476 **9. Mechanism and implication for deglacial atmospheric CO_2 rise**

477 Our inferred erosion of the spatial isolation of deep water masses during HS1
478 is roughly coeval with the intensified upwelling and breakdown of deep vertical
479 stratification in the Southern Ocean during the rapid warming in Antarctica (Fig. 4E,
480 I) (Anderson et al., 2009; Barbante et al., 2006). The synchronicity of these events
481 suggests that they may be linked to one another by a common mechanism. Northern

Hemisphere insolation-induced fresh water input into the North Atlantic at last glacial termination led to a reduction of NADW formation during HS1 (Fig. 4A) (He et al., 2013; Liu et al., 2009; McManus et al., 2004). Through atmospheric teleconnections, a NADW shutdown may also cause poleward displacement or strengthening of the Southern Hemisphere westerlies (McGlone et al., 2010; Putnam et al., 2010), as invoked previously to account for increased opal fluxes in the Southern Ocean (Fig. 4E) (Anderson et al., 2009). Changes in the southern westerlies may have increased lateral (zonal) exchange of deep waters around Antarctica (Ho et al., 2012) through more efficient transfer of momentum from the winds to the ocean at the critical latitudes of the Drake Passage (Toggweiler et al., 2006), while also enhancing the meridional overturning in the Southern Ocean via Ekman pumping (Anderson et al., 2009; Morrison and Hogg, 2013; Toggweiler et al., 2006) (Fig. 6).

The deep Pacific Ocean stores the largest amount of carbon in the ocean-land biosphere-atmosphere system today (Broecker, 1982; Key et al., 2004), and proxies suggest an even larger carbon stock in the deep Pacific during the LGM (Bradtmiller et al., 2010; Jaccard and Galbraith, 2012). Reduced glacial interocean mixing would have facilitated storage of low-[CO_3^{2-}], old-^{14}C, low-O_2 (Bradtmiller et al., 2010; Galbraith et al., 2007; Jaccard and Galbraith, 2012) and, presumably, high-DIC waters in the deep Pacific Ocean (Fig. 1, 4B-D), contributing to low atmospheric CO_2 during the LGM (Fig. 4H) (Monnin et al., 2001). Whatever the nature of the physical processes responsible for increased lateral mixing during HS1, they must have contributed to the ventilation of CO_2 from the deep Pacific. Interocean exchange of deep waters is constrained to occur via the Southern Ocean, where enhanced vertical mixing during HS1 was recorded by the burial flux of biogenic opal (Fig. 4E)

(Anderson et al., 2009). Consequently, it is reasonable to infer that a portion, although not necessarily all, of the deep water exchanging between the South Atlantic and Pacific Oceans was subject to entrainment by the processes driving vertical mixing, thereby enhancing the ventilation of DIC previously stored in deep Pacific waters.

Geochemical tracers cannot be used to quantify the relative contributions by vertical and lateral deep water exchange to the deglacial increase in deep ocean ventilation, but they inform us that both occurred. Recent modeling suggests that transport by the Antarctic Circumpolar Current (ACC; linked to lateral deepwater exchange) is much less sensitive to changes in the southern westerlies than is meridional overturning circulation (Morrison and Hogg, 2013). However, the westerlies in their model runs are in a modern poleward-shifted position, under which condition ACC is possibly in an eddy-saturated state. By contrast, the transition from the LGM to HS1 might involve a much larger poleward shift in the position of the westerlies (possibly beginning from a position during the LGM equatorward of their modern location), which could impose a stronger impact on Southern Ocean hydrography. In light of the compelling evidence for homogenization of deep waters during HS1, and the implications for understanding climate-related changes in atmospheric CO_2, we hope that our findings will encourage investigators to dig deeper into the processes involved and help reconcile the physical oceanographic models with paleoceanograhic observations.

10. Conclusion

Using a high-resolution reconstruction of [CO_3^{2-}] in the deep South Atlantic, we describe the sequence of events that shaped the ocean carbon cycle and atmospheric CO_2 since the last ice age. During the initial phase of deglaciation, increased lateral exchange of deep water between the Pacific and Atlantic Oceans enhanced the ventilation of CO_2 from the deep sea by the contemporary intensification of vertical mixing. The initial chemical signature of North Atlantic Deep Water occurred during the Bølling (~14.5 kyr), while the principal Holocene feature of the record indicates extraction of alkalinity from seawater by $CaCO_3$ deposition on continental shelves. Our study provides an unprecedented high-resolution deep water [CO_3^{2-}] record in the South Atlantic to improve our understanding of the global carbon cycle in the past.

Acknowledgments

Core material used in this study was provided by the Lamont-Doherty Earth Observatory Deep-sea Sample Repository. We thank W.S. Broecker, X. Wang, P. De Deckker, S. Eggins, and B. Opdyke for discussions, P. Tomascak, B. Yan, and P. Wang for laboratory assistance, and Robbie Toggweiler and two anonymous reviewers for comments. This work is supported by ARC DP140101393, the Lawrence Livermore National Laboratory's Lawrence Fellowship Program, a Lamont-Doherty Postdoctoral Fellowship, and a Comer Science and Education Foundation Fellowship (JY), and the CAS/SAFEA International Partnership Program for Creative Research Teams (JY/ZJ), the US NSF (RFA; OCE 0823507), and contribution from Laureate Fellowship FL120100050 (EJR).

Author contributions

J.Y. designed and managed the project and measured B/Ca. R.F.A. measured Th-U. J.Y. and R.F.A. developed interpretation and wrote the manuscript with assistance from all authors. Z.J. and F.Z. picked and prepared benthic foraminifera for B/Ca and ^{14}C dating. All authors commented on the manuscript.

560

561 **References**

562 Anderson, D.M., Archer, D., 2002. Glacial-interglacial stability of ocean pH inferred from
563 foraminifer dissolution rates. Nature 416, 70-73.

564 Anderson, R.F., Ali, S., Bradtmiller, L., Nielsen, S.H.H., Fleisher, M.Q., Anderson, B.E.,
565 Burckle, L.H., 2009. Wind-driven upwelling in the Southern Ocean and the deglacial rise in
566 atmospheric CO_2. Science 323, 1443-1448.

567 Anderson, R.F., Fleisher, M.Q., Lao, Y., Winckler, G., 2008. Modern $CaCO_3$ preservation in
568 equatorial Pacific sediments in the context of late-Pleistocene glacial cycles. Mar. Chem.,
569 doi:10.1016/j.marchem.2007.1011.1011.

570 Barbante, C., Barnola, J.M., Becagli, S., Beer, J., Bigler, M., Boutron, C., Blunier, T.,
571 Castellano, E., Cattani, O., Chappellaz, J., Dahl-Jensen, D., Debret, M., Delmonte, B., Dick,
572 D., Falourd, S., Faria, S., Federer, U., Fischer, H., Freitag, J., Frenzel, A., Fritzsche, D.,
573 Fundel, F., Gabrielli, P., Gaspari, V., Gersonde, R., Graf, W., Grigoriev, D., Hamann, I.,
574 Hansson, M., Hoffmann, G., Hutterli, M.A., Huybrechts, P., Isaksson, E., Johnsen, S., Jouzel,
575 J., Kaczmarska, M., Karlin, T., Kaufmann, P., Kipfstuhl, S., Kohno, M., Lambert, F.,
576 Lambrecht, A., Lambrecht, A., Landais, A., Lawer, G., Leuenberger, M., Littot, G.,
577 Loulergue, L., Luthi, D., Maggi, V., Marino, F., Masson-Delmotte, V., Meyer, H., Miller, H.,
578 Mulvaney, R., Narcisi, B., Oerlemans, J., Oerter, H., Parrenin, F., Petit, J.R., Raisbeck, G.,
579 Raynaud, D., Rothlisberger, R., Ruth, U., Rybak, O., Severi, M., Schmitt, J., Schwander, J.,
580 Siegenthaler, U., Siggaard-Andersen, M.L., Spahni, R., Steffensen, J.P., Stenni, B., Stocker,
581 T.F., Tison, J.L., Traversi, R., Udisti, R., Valero-Delgado, F., van den Broeke, M.R., van de
582 Wal, R.S.W., Wagenbach, D., Wegner, A., Weiler, K., Wilhelms, F., Winther, J.G., Wolff, E.,
583 Members, E.C., 2006. One-to-one coupling of glacial climate variability in Greenland and
584 Antarctica. Nature 444, 195-198. 10.1038/Nature05301

585 Barker, S., Diz, P., vautravers, M., Pike, J., Knorr, G., Hall, I.R., Broecker, W., 2009.
586 Interhemispheric Atlantic seesaw response during the last deglaciation. Nature 457, 1097-
587 1102.

588 Barker, S., Greaves, M., Elderfield, H., 2003. A study of cleaning procedures used for
589 foraminiferal Mg/Ca paleothermometry. Geochem. Geophys. Geosyst. 4, 8407.
590 doi:10.1029/2003GC000559

591 Barker, S., Knorr, G., Vautravers, M., Diz, P., Skinner, L., 2010. Extreme deepening of the
592 Atlantic overturning circulation during deglaciation. Nature Geoscience 3, 567-571.

593 Bianchi, C., Gersonde, R., 2004. Climate evolution at the last deglaciation: the role of the
594 Southern Ocean. Earth Planet. Sci. Lett. 228, 407-424. 10.1016/j.epsl.2004.10.003

595 Bradtmiller, L., Anderson, R.F., Sachs, J., Fleisher, M.Q., 2010. A deeper respired carbon
596 pool in the glacial equatorial Pacific Ocean. Earth Planet. Sci. Lett.,
597 doi:10.1016/j.epsl.2010.1009.1022.

598 Broecker, W., 1982. Glacial to interglacial changes in ocean chemistry. Progr. Oceanogr. 2,
599 151-197.

600 Broecker, W., Clark, E., Barker, S., Hajdas, I., Bonani, G., Moreno, E., 2007. Radiocarbon
601 age of late glacial deep water from the equatorial Pacific. Paleoceanogr. 22, PA2206,
602 doi:2210.1029/2006PA001359.

603 Broecker, W., Maier-Reimer, E., 1992. The influence of air and sea exchange on the carbon
604 isotope distribution in the sea. Glob. Biogeochem. Cycle 6, 315-320.

Broecker, W., Putnam, A.E., 2012. How did the hydrologic cycle respond to the two-phase mystery interval? Quat. Sci. Rev. 57, 17-25. DOI 10.1016/j.quascirev.2012.09.024

Broecker, W.S., Peng, T.H., 1987. The role of $CaCO_3$ compensation in the glacial to interglacial atmospheric CO_2 change. Glob. Biogeochem. Cycle 1, 15-29.

Brown, R.E., Anderson, L.D., Thomas, E., Zachos, J.C., 2011. A core-top calibration of B/Ca in the benthic foraminifers Nuttallides umbonifera and Oridorsalis umbonatus: A proxy for Cenozoic bottom water carbonate saturation. Earth Planet. Sci. Lett. 310, 360-368. 10.1016/j.epsl.2011.08.023

Burke, A., Robinson, L.F., 2012. The Southern Ocean's role in carbon exchange during the last deglaciation. Science, doi:10.1126/science.1208163.

Charles, C.D., Fairbanks, R.G., 1992. Evidence from Southern-Ocean Sediments for the Effect of North-Atlantic Deep-Water Flux on Climate. Nature 355, 416-419. 10.1038/355416a0

Corliss, B.H., 1985. Microhabitats of benthic foraminifera within deep-sea sediments. Nature 314, 435-438.

Curry, W.B., Oppo, D., 2005. Glacial water mass geometry and the distribution of $\delta^{13}C$ of ΣCO_2 in the western Altantic Ocean. Paleoceanogr. 20, PA1017, doi:1010.1029/2004PA001021.

Divine, D.V., Koc, N., Isaksson, E., Nielsen, S., Crosta, X., Godtliebsen, F., 2010. Holocene Antarctic climate variability from ice and marine sediment cores: Insights on ocean-atmosphere interaction. Quat. Sci. Rev. 29, 303-312. 10.1016/j.quascirev.2009.11.012

Elsig, J., Schmitt, J., Leuenberger, D., Schneider, R.R., Eyer, M., Leuenberger, M., Joos, F., Fischer, H., Stocker, T.F., 2009. Stable isotope constraints on Holocene carbon cycle changes from an Antarctic ice core. Nature 461, 507-510.

Farrell, J.W., Prell, W.L., 1989. Climatic change and $CaCO_3$ preservation: an 800,000 year bathymetric reconstruction from the central equatorial Pacific Ocean. Paleoceanogr. 4, 447-466.

Fleisher, M.Q., Anderson, R.F., 2003. Assessing the collection efficiency of Ross Sea sediment traps using Th-230 and Pa-231. Deep-Sea Research Part Ii-Topical Studies in Oceanography 50, 693-712. Pii S0967-0645(02)00591-X

Doi 10.1016/S0967-0645(02)00591-X

Foster, G.L., 2008. Seawater pH, pCO_2 and $[CO_3^{2-}]$ variations in the Caribbean Sea over the last 130 kyr; a boron isotope and B/Ca study of planktic foraminifera. Earth Planet. Sci. Lett. 271, 254-266. doi: 210.1016/j.epsl.2008.1004.1015.

Galbraith, E.D., Jaccard, S.L., Pedersen, T.F., Sigman, D.M., Haug, G.H., Cook, M., Southon, J.R., Francois, R., 2007. Carbon dioxide release from the North Pacific abyss during the last deglaciation. Nature 449, 890-893.

He, F., Shakun, J.D., Clark, P.U., Carlson, A.E., Liu, Z.Y., Otto-Bliesner, B.L., Kutzbach, J.E., 2013. Northern Hemisphere forcing of Southern Hemisphere climate during the last deglaciation. Nature 494, 81-85. Doi 10.1038/Nature11822

Ho, S.L., Mollenhauer, G., Lamy, F., Martinez-Garcia, A., Mohtadi, M., Gersonde, R., Hebbeln, D., Nunez-Ricardo, S., Rosell-Mele, A., Tiedemann, R., 2012. Sea surface temperature variability in the Pacific sector of the Southern Ocean over the past 700 kyr. Paleoceanogr. 27. Artn Pa4202, 10.1029/2012pa002317

Hodell, D.A., Charles, C.D., Sierro, F.J., 2001. Late Pleistocene evolution of the ocean's carbonate system. Earth Planet. Sci. Lett. 192, 109-124.

Howard, W.R., Prell, W.L., 1994. Late Quaternary $CaCO_3$ production and preservation in the Southern Ocean - Implications for oceanic and atmospheric carbon cycling. Paleoceanogr. 9, 453-482.

Jaccard, S.L., Galbraith, E.D., 2012. Large climate-driven changes of oceanic oxygen concentrations during the last deglaciation. Nature Geoscience 5, 151-156. 10.1038/Ngeo1352

Karlin, R., Lyle, M., Zahn, R., 1992. Carbonate Variations in the Northeast Pacific during the Late Quaternary. Paleoceanogr. 7, 43-61. Doi 10.1029/91pa03077

Key, R.M., Kozyr, A., Sabine, C.L., Lee, K., Wanninkhof, R., Bullister, J.L., Feely, R.A., Millero, F.J., Mordy, C., Peng, T.H., 2004. A global ocean carbon climatology: Results from Global Data Analysis Project (GLODAP). Glob. Biogeochem. Cycle 18. 10.1029/2004GB002247

Lea, D., Bijam, J., Spero, H., Archer, D., 1999. Implications of a carbonate ion effect on shell carbon and oxygen isotopes for glacial ocean conditions, In: Fischer, G., Wefer, G. (Eds.), Use of Proxies in Paleoceanography: Examples from the South Atlantic. Springer-Verlag, Berlin Heidelberg, pp. 513-522.

Lemieux-Dudon, B., Blayo, E., Petit, J.R., Waelbroeck, C., Svensson, A., Ritz, C., Barnola, J.M., Narcisi, B.M., Parrenin, F., 2010. Consistent dating for Antarctic and Greenland ice cores. Quat. Sci. Rev. 29, 8-20.

Liu, Z., Otto-Bliesner, B.L., He, F., Brady, E.C., Tomas, R., Clark, P.U., Carlson, A.E., Lynch-Stieglitz, J., Curry, W., Brook, E., Erickson, D., Jacob, R., Kutzbach, J., Cheng, J., 2009. Transient Simulation of Last Deglaciation with a New Mechanism for Bolling-Allerod Warming. Science 325, 310-314. DOI 10.1126/science.1171041

Lund, D.C., Adkins, J.F., Ferrari, R., 2011. Abyssal Atlantic circulation during the Last Glacial Maximum: Constraining the ratio between transport and vertical mixing. Paleoceanogr. 26. 10.1029/2010pa001938

Lutze, G.F., Thiel, H., 1989. Epibenthic foraminifera from elevated microhabitats: *Cibicidoides wuellerstorfi* and *Planulina ariminensis*. J. Foraminiferal Res. 19, 153-158.

Lyle, M., Mix, A.C., Ravelo, A.C., Andreasen, D., Heuser, L., Olivarez, A., 2000. Millennial-scale $CaCO_3$ and C_{org} events along the Northern and central California margins: stratigraphy and origins, In: Lyle, M., Koizumi, I., Richter, C., Moore, T.C. (Eds.), Proceedings of the Ocean Drilling Program, Scientific Results, pp. 163-182.

Mackensen, A., 2012. Strong thermodynamic imprint on Recent bottom-water and epibenthic delta C-13 in the Weddell Sea revealed: Implications for glacial Southern Ocean ventilation. Earth Planet. Sci. Lett. 317, 20-26. DOI 10.1016/j.epsl.2011.11.030

Mackensen, A., Hubberten, H.-W., Bickert, T., Fischer, G., Fütterer, D.K., 1993. The $\delta^{13}C$ in benthic foraminiferal tests of *Fontbotia wuellerstorfi* (schwager) relative to the $\delta^{13}C$ of dissolved inorganic carbon in Souther Ocean deep water: Implications for glacial ocean circulation models. Paleoceanogr. 8, 587-610.

McCave, I.N., Carter, L., Hall, I.R., 2008. Glacial-interglacial changes in water mass structure and flow in the SW Pacific Ocean. Quat. Sci. Rev. 27, 1886-1908. 10.1016/j.quascirev.2008.07.010

McGlone, M.S., Turney, C.S.M., Wilmshurst, J.M., Renwick, J., Pahnke, K., 2010. Divergent trends in land and ocean temperature in the Southern Ocean over the past 18,000 years. Nature Geoscience 3, 622-626. 10.1038/Ngeo931

McManus, J., Francois, R., Gherardi, J.-M., Keigwin, L., Brown-Leger, S., 2004. Collapse and rapid resumption of Atlantic meridional circulation linked to deglacial climate changes. Nature 428, 834-837.

699 Menviel, L., Joos, F., 2012. Toward explaining the Holocene carbon dioxide and carbon
700 isotope records: Results from transient ocean carbon cycle-climate simulations. Paleoceanogr.
701 27. 10.1029/2011pa002224

702 Menviel, L., Timmermann, A., Timm, O.E., Mouchet, A., 2011. Deconstructing the Last
703 Glacial termination: the role of millennial and orbital-scale forcings. Quat. Sci. Rev. 30, 1155-
704 1172. 10.1016/j.quascirev.2011.02.005

705 Monnin, E., Indermuhle, A., Dällenbach, A., Fluckiger, J., Stauffer, B., Stocker, T.F.,
706 Raynaud, D., Barnola, J.M., 2001. Atmospheric CO_2 Concentrations over the Last Glacial
707 Termination. Science 291, 112-114.

708 Morrison, A.K., Hogg, A.M., 2013. On the Relationship between Southern Ocean
709 Overturning and ACC Transport. J Phys Oceanogr 43, 140-148. Doi 10.1175/Jpo-D-12-057.1

710 Ninnemann, U.S., Charles, C.D., 2002. Changes in the mode of Southern Ocean circulation
711 over the last glacial cycle revealed by foraminiferal stable isotopic variability. Earth Planet.
712 Sci. Lett. 201, 383-396.

713 Opdyke, B.N., Walker, J.C.G., 1992. Return of the Coral-Reef Hypothesis - Basin to Shelf
714 Partitioning of $CaCO_3$ and Its Effect on Atmospheric CO_2. Geology 20, 733-736.

715 Piotrowski, A., Galy, A., Nicholl, J.A.L., Roberts, N., Wilson, D.J., Clegg, J.A., Yu, J., 2012.
716 Reconstructing deglacial North and South Atlantic deep water sourcing using foraminiferal
717 Nd isotopes. Earth Planet. Sci. Lett. 357-358, 289-297.

718 Piotrowski, A., Goldstein, S.J., Hemming, S.R., Fairbanks, R.G., 2005. Temporal
719 Relationships of carbon cycling and ocean circulation at glacial boundaries. Science 307,
720 1933-1938.

721 Putnam, A.E., Denton, G.H., Schaefer, J.M., Barrell, D.J.A., Andersen, B.G., Finkel, R.C.,
722 Schwartz, R., Doughty, A.M., Kaplan, M.R., Schluchter, C., 2010. Glacier advance in
723 southern middle-latitudes during the Antarctic Cold Reversal. Nature Geoscience 3, 700-704.
724 10.1038/Ngeo962

725 Rae, J.W.B., Foster, G.L., Schmidt, D.N., Elliott, T., 2011. Boron isotopes and B/Ca in
726 benthic foraminifera: Proxies for the deep ocean carbonate system. Earth Planet. Sci. Lett.
727 302, 403-413. 10.1016/j.epsl.2010.12.034

728 Raitzsch, M., Hathorne, E.C., Kuhnert, H., Groeneveld, J., Bickert, T., 2011. Modern and late
729 Pleistocene B/Ca ratios of the benthic foraminifer Planulina wuellerstorfi determined with
730 laser ablation ICP-MS. Geology 39, 1039-1042. 10.1130/G32009.1

731 Reimer, P.J., Baillie, M.G.L., Bard, E., Bayliss, A., Beck, J.W., Blackwell, P.G., Ramsey,
732 C.B., Buck, C.E., Burr, G.S., Edwards, R.L., Friedrich, M., Grootes, P.M., Guilderson, T.P.,
733 Hajdas, I., Heaton, T.J., Hogg, A.G., Hughen, K.A., Kaiser, K.F., Kromer, B., McCormac,
734 F.G., Manning, S.W., Reimer, R.W., Richards, D.A., Southon, J.R., Talamo, S., Turney,
735 C.S.M., van der Plicht, J., Weyhenmeyer, C.E., 2009. Intcal09 and Marine09 radiocarbon age
736 calibration curves, 0-50,000 years cal BP. Radiocarbon 51, 1111-1150.

737 Rickaby, R.E.M., Elderfield, H., Roberts, N., Hillenbrand, C.-D., Mackensen, A., 2010.
738 Evidence for elevated alkalinity in the glacial Southern Ocean. Paleoceanogr. 25, PA1209,
739 doi:1210.1029/2009PA001762.

740 Ridgwell, A.J., Watson, A.J., Maslin, M.A., Kaplan, J.O., 2003. Implications of coral reef
741 buildup for the controls on atmospheric CO_2 since the Last Glacial Maximum. Paleoceanogr.
742 18. 10.1029/2003PA000893

743 Sachs, J.P., Anderson, R.F., 2003. Fidelity of alkenone paleotemperatures in southern Cape
744 Basin sediment drifts. Paleoceanogr. 18. Artn 1082, Doi 10.1029/2002pa000862

Schmitt, J., Schneider, R., Elsig, J., Leuenberger, D., Lourantou, A., Chappellaz, J., Kohler, P., Joos, F., Stocker, T.F., Leuenberger, M., Fischer, H., 2012. Carbon isotope constraints on the deglacial CO_2 rise from ice cores. Science, doi 10.1126/science.1217161.

Sigman, D.M., Boyle, E.A., 2000. Glacial/interglacial variations in atmospheric carbon dioxide. Nature 407, 859-869.

Sigman, D.M., Hain, M.P., Haug, G.H., 2010a. The polar ocean and glacial cycles in atmospheric CO_2 concentration. Nature 466, 47-55.

Sigman, D.M., Hain, M.P., Haug, G.H., 2010b. The polar ocean and glacial cycles in atmospheric CO_2 concentration. Nature 466, 47-55. 10.1038/Nature09149

Skinner, L., Fallon, S.J., Waelbroeck, C., Michel, E., Barker, S., 2010. Ventilation of the Deep Southern Ocean and Deglacial CO_2 Rise. Science 328, 1147-1151.

Stuiver, M., Reimer, P.J., 1993. Extended ^{14}C data-base and revised Calib 3.0 14C age calibration program. Radiocarbon 35, 215-230.

Toggweiler, J.R., Russell, J.L., Carson, S.R., 2006. Midlatitude westerlies, atmospheric CO_2, and climate change during the ice ages. Paleoceanogr. 21, PA2005, doi:2010.1029/2005PA001154, 002006.

Vecsei, A., Berger, W.H., 2004. Increase of atmospheric CO_2 during deglaciation: Constraints on the coral reef hypothesis from patterns of deposition. Glob. Biogeochem. Cycle 18. 10.1029/2003gb002147

Yu, J., Anderson, R.F., Jin, Z.D., Rae, J., Opdyke, B.N., Eggins, S., 2013a. Responses of the deep ocean carbonate system to carbon reorganization during the Last Glacial–interglacial cycle. Quat. Sci. Rev. 76, 39-52. http://dx.doi.org/10.1016/j.quascirev.2013.06.020

Yu, J., Broecker, W., Elderfield, H., Jin, Z.D., McManus, J., Zhang, F., 2010a. Loss of carbon from the deep sea since the Last Glacial Maximum. Science 330, 1084-1087, doi: 1010.1126/science.1193221.

Yu, J., Foster, G.L., Elderfield, H., Broecker, W.S., Clark, E., 2010b. An evaluation of benthic foraminiferal B/Ca and delta(11)B for deep ocean carbonate ion and pH reconstructions. Earth Planet. Sci. Lett. 293, 114-120. 10.1016/j.epsl.2010.02.029

Yu, J., Thornalley, D.J.R., Rae, J., McCave, I.N., 2013b. Calibration and application of B/Ca, Cd/Ca, and $\delta^{11}B$ in *Neogloboquadrina pachyderma* (sinistral) to constrain CO_2 uptake in the subpolar North Atlantic during the last deglaciation. Paleoceanogr. 10.1002/palo.20024

Yu, J.M., Day, J., Greaves, M., Elderfield, H., 2005. Determination of multiple element/calcium ratios in foraminiferal calcite by quadrupole ICP-MS. Geochem. Geophys. Geosyst. 6, Q08P01, doi:10.1029/2005GC000964.

Yu, J.M., Elderfield, H., 2007. Benthic foraminiferal B/Ca ratios reflect deep water carbonate saturation state. Earth Planet. Sci. Lett. 258, 73-86, doi: 10.1016/j.epsl.2007.1003.1025.

Yu, J.M., Elderfield, H., Greaves, M., Day, J., 2007. Preferential dissolution of benthic foraminiferal calcite during laboratory reductive cleaning. Geochem. Geophys. Geosyst. 8, Q06016, doi:06010.01029/02006GC001571.

Yu, J.M., Elderfield, H., Piotrowski, A., 2008. Seawater carbonate ion-$\delta^{13}C$ systematics and application to glacial-interglacial North Atlantic ocean circulation. Earth Planet. Sci. Lett. 271, 209-220. doi:210.1016/j.epsl.2008.1004.1010.

Yu, J.M., Foster, G.L., Elderfield, H., Broecker, W.S., Clark, E., 2010c. An evaluation of benthic foraminiferal B/Ca and $\delta^{11}B$ for deep ocean carbonate ion and pH reconstructions. Earth Planet. Sci. Lett. 293, 114-120, 110.1016/j.epsl.2010.1002.1029

Figure Legends,

Fig. 1. Locations of core TNO57-21 and two cores in the Western Equatorial Pacific (WEP) against the pre-industrial seawater [CO_3^{2-}]. Inset shows the locations of hydrographic sites used for the [CO_3^{2-}] section (Key et al., 2004). The map was generated using Ocean Data View (http://odv.awi-bremerhaven.de.). Three key water masses are indicated: NADW = North Atlantic Deep Water, LCDW = Lower Circumpolar Deep Water, and NPDW = North Pacific Deep Water.

Fig. 2. Data from core TNO57-21. (A) *C. wuellerstorfi* B/Ca and reconstructed deep water [CO_3^{2-}] (red circles) with b-spline smoothing (red curve). The error bar represents the average 2σ [CO_3^{2-}] error from analytical uncertainty in B/Ca. (B) %$CaCO_3$ (green crosses) and ^{230}Th-normalized $CaCO_3$ flux (blue squares) (Sachs and Anderson, 2003; this study). (C) benthic $\delta^{13}C$ (Ninnemann and Charles, 2002). Triangles at the bottom represent new (Table S1) and published (Barker et al., 2010) radiocarbon dates.

Fig. 3. Vertical seawater [CO_3^{2-}] distributions during the LGM and today. LGM data are for the North Atlantic (Yu et al., 2010a), equatorial (EQ) Atlantic (Raitzsch et al., 2011), South Atlantic (this study), and Indo-Pacific Oceans (Yu et al., 2013a; Yu et al., 2010a). Error bars represent 1 standard deviation of values from the LGM. Modern global seawater [CO_3^{2-}] is from the eWOCE dataset (http://www.ewoce.org/). Squares along the top x-axis represent surface water [CO_3^{2-}] reconstructions for the tropical Atlantic during the Holocene and the LGM (Foster, 2008). Little change in

814 deep Indo-Pacific [CO_3^{2-}] is also supported by foraminiferal assemblage analyses
815 (Anderson and Archer, 2002).

816

817 **Fig. 4**. Marine and atmospheric records over the past 28 kyr. (A) North Atlantic Deep
818 Water formation strength from Pa/Th (McManus et al., 2004). (B) [CO_3^{2-}] at TNO57-
819 21 (this study) and GGC48 (Yu et al., 2010a). (C) Benthic $\delta^{13}C$ at TNO57-
820 21(Ninnemann and Charles, 2002) and GGC48 (Yu et al., 2010a). (D) $\Delta\Delta^{14}C$, the
821 benthic-atmospheric $\Delta^{14}C$ offset, for TNO57-21 (Barker et al., 2010) and MD01-2386
822 (Broecker et al., 2007). In (B-D), red solid circles are for TNO57-21, while green
823 empty symbols are for WEP cores. (E) Opal flux in the Antarctic Zone (Anderson et
824 al., 2009). (F) atmospheric $\Delta^{14}C$ (Reimer et al., 2009). (G) atmospheric $\delta^{13}CO_2$
825 (Schmitt et al., 2012). (H) atmospheric CO_2 (Monnin et al., 2001). (I) EDML ice core
826 $\delta^{18}O$ (Barbante et al., 2006). Ice core data are on the age model of (Lemieux-Dudon et
827 al., 2010). Error bars in (B, C, F, G) are 1σ uncertainties, the ellipse in (D) represents
828 approximate average 2σ error, and curves in (B, G) are b-spline smoothing. Triangles
829 at base represent radiocarbon dates for TNO57-21 (SI Text) (Barker et al., 2010).

830

831 **Fig. 5.** Bathymetric distributions of $\delta^{13}C$ during the LGM (A) and today (B). The
832 large $\delta^{13}C$ dissimilarity shown in (A) suggests a poorly mixed deep ocean during the
833 LGM. This is in stark contrast to much reduced $\delta^{13}C$ variability in the modern ocean
834 (B), where deep waters are well mixed. There must have been an increase in lateral
835 exchange of deep water from the LGM to today. Our data (Fig. 4) explain when (HS1)
836 and how (increased lateral mixing) this increase occurred, and provide new insights

837 into the global carbon cycle during the last deglaciation. Data source: LGM benthic
838 $\delta^{13}C$ (curves in A) are from (McCave et al., 2008) and references therein; modern
839 hydrographic data are compiled in the eWOCE dataset (http://www.ewoce.org/) and
840 are for sites (curves in B) close to the locations of cores used for the LGM profile
841 reconstructions in (A): S Atlantic - sites 7320/16288 (11.5^{o}E, 49.6^{o}S), S Indian - sites
842 7516/7522 (57.9^{o}E, 47.7^{o}S), S. Pacific - sites 11724/11727/7426 (175.9^{o}E, 30.9^{o}S),
843 EQ Pacific - site 11690 (165^{o}E, 0^{o}N). LGM and Holocene averages for cores GGC48
844 and TNO57-21 are shown by blue circles and red squares with error bars representing
845 1 standard deviation of values from the designated age intervals, respectively.

846

847

848 **Fig. 6.** Schematic illustration of processes affecting deglacial interocean deep water
849 exchange and CO_2 degassing. (A) LGM. (B) HS1. Compared to the LGM, deep South
850 Atlantic-Pacific carbon exchange during HS1 was enhanced by increased meridional
851 (isopycnal) mixing (Morrison and Hogg, 2013) and by increased Antarctic
852 Circumpolar Current flow (Ho et al., 2012), probably due to a poleward shift and/or
853 intensification of Southern Westerlies (Anderson et al., 2009; Toggweiler et al.,
854 2006). By distributing CO_2-rich deep Pacific waters around Antarctica, increased
855 interocean mixing would have augmented CO_2 degassing in the Southern Ocean
856 during the breakdown of vertical stratification (Anderson et al., 2009; Burke and
857 Robinson, 2012; Sigman et al., 2010b) and sea ice retreat (Bianchi and Gersonde,
858 2004; Divine et al., 2010) during HS1. Thicker lines indicate increased fluxes or wind
859 stress. Figure is modified from Charles and Fairbanks (1992).

860

Figures

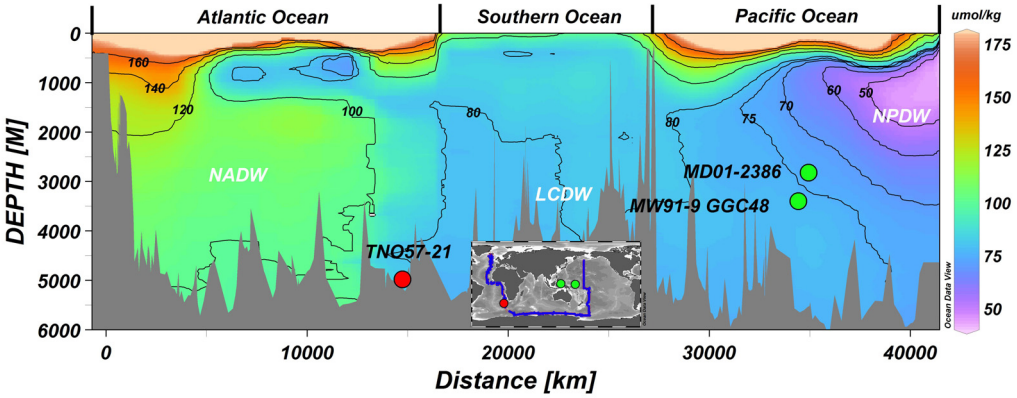

Fig. 1

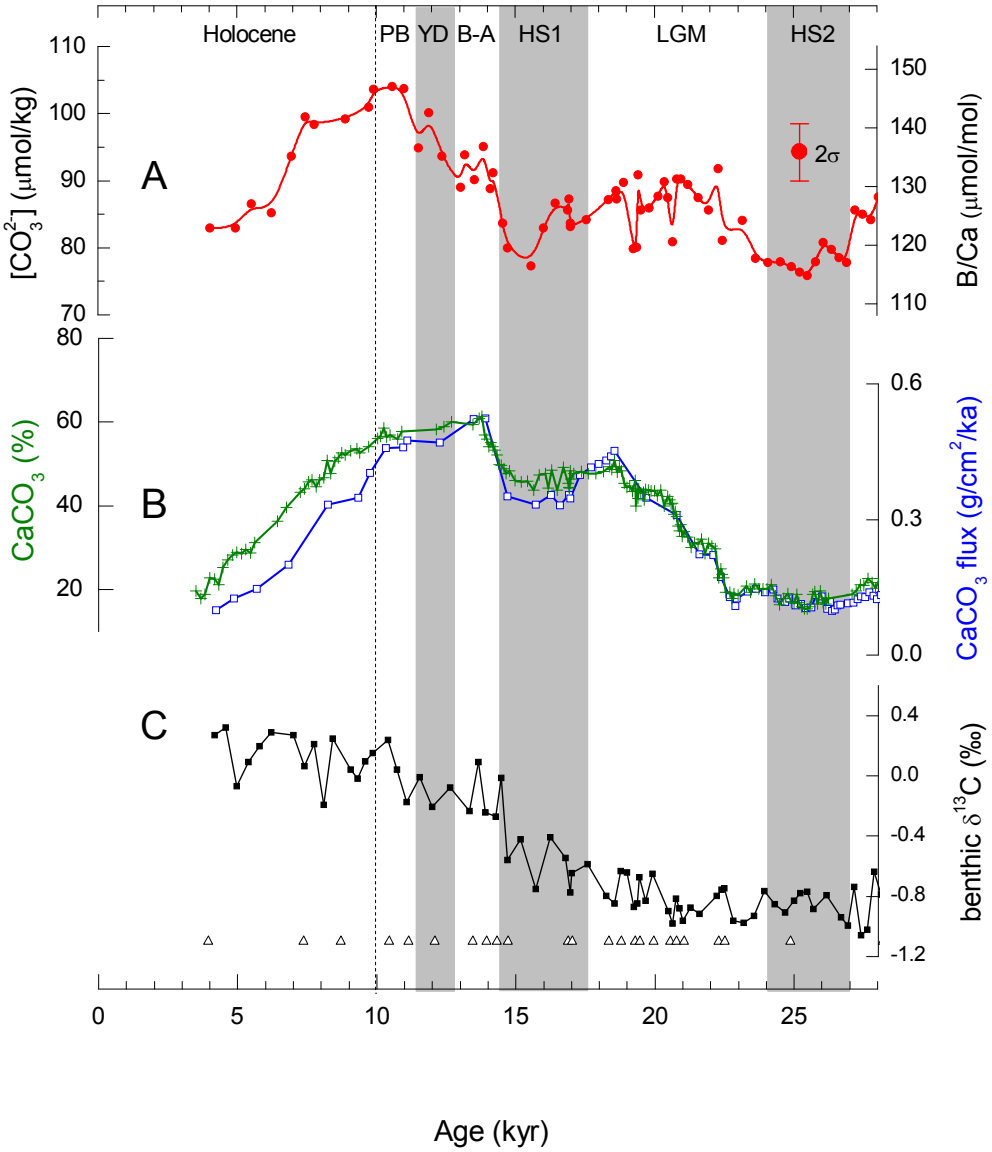
Holocene
PB
YD
B-A
HS1
LGM
HS2
A
B
C
2σ
[CO3 2-] (µmol/kg)
B/Ca (µmol/mol)
CaCO3 (%)
CaCO3 flux (g/cm2/ka)
benthic δ13C (‰)
Age (kyr)

Fig. 2

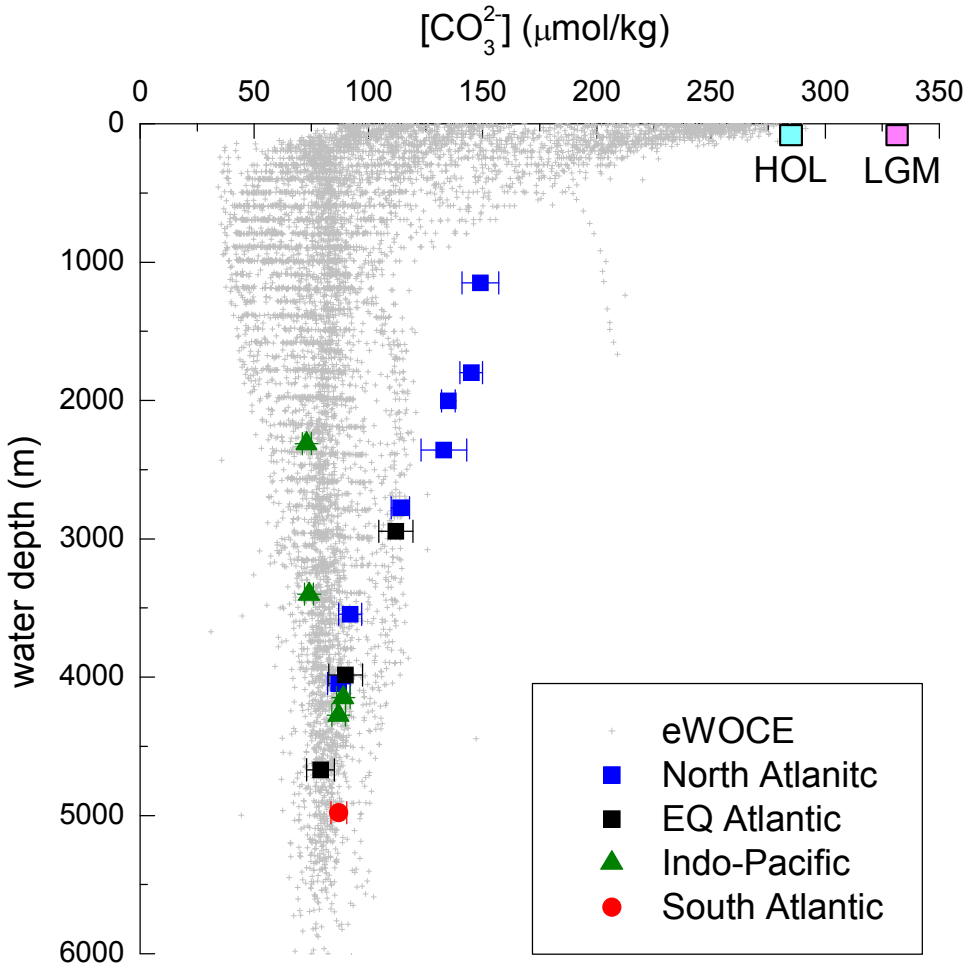
[CO3 2-] (μmol/kg)
0
50
100
150
200
250
300
350
0
1000
2000
3000
4000
5000
6000
water depth (m)
HOL
LGM
eWOCE
North Atlanitc
EQ Atlantic
Indo-Pacific
South Atlantic

Fig. 3

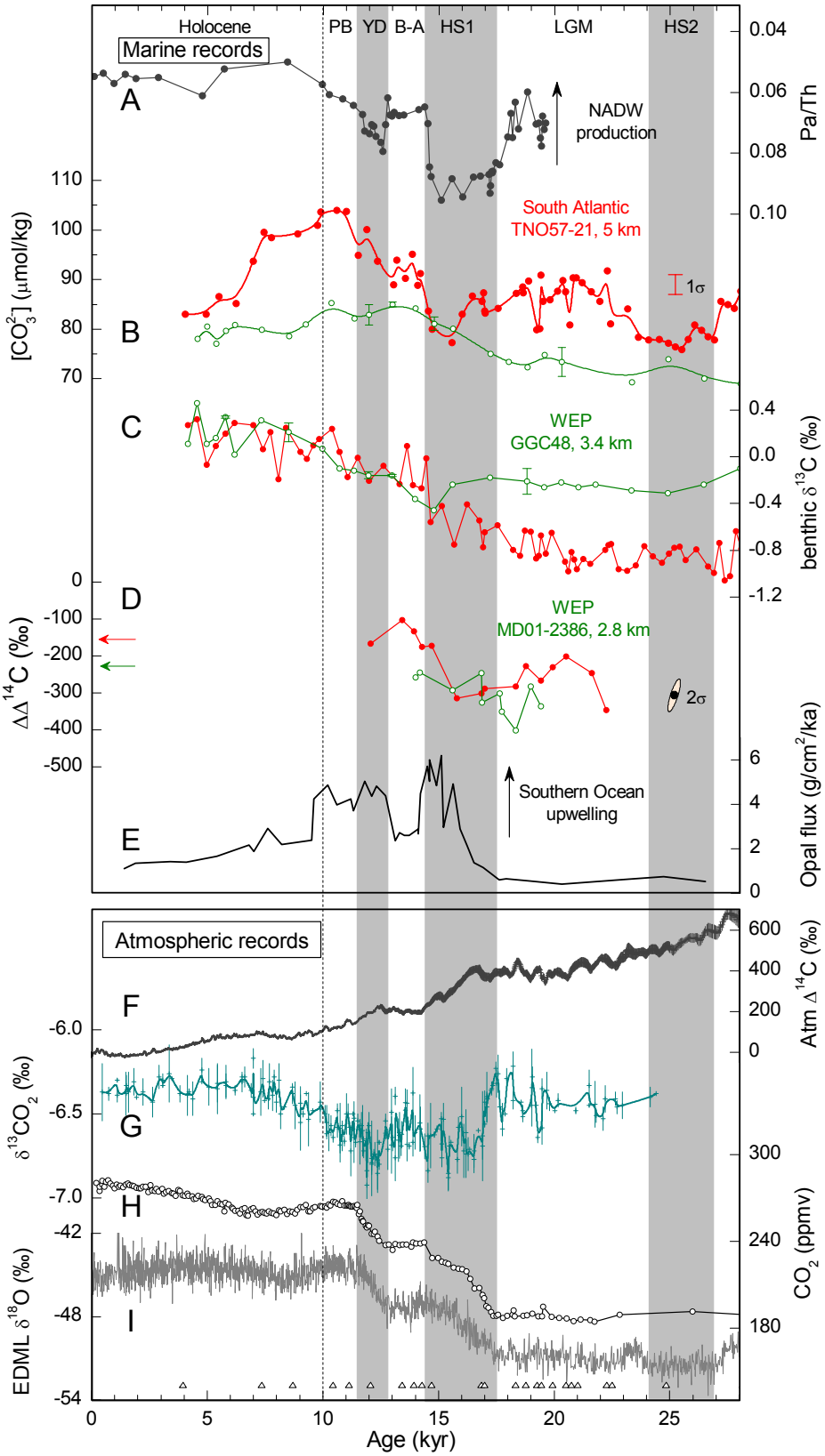
Holocene
PB
YD
B-A
HS1
LGM
HS2
Marine records
A
NADW
production
Pa/Th
0.04
0.06
0.08
0.10
110
100
90
80
70
[CO3 2-] (µmol/kg)
South Atlantic
TNO57-21, 5 km
1σ
B
C
WEP
GGC48, 3.4 km
0.4
0.0
-0.4
-0.8
-1.2
benthic δ13C (‰)
0
-100
-200
-300
-400
-500
ΔΔ14C (‰)
D
WEP
MD01-2386, 2.8 km
2σ
6
4
2
0
Opal flux (g/cm2/ka)
Southern Ocean
upwelling
E
Atmospheric records
F
600
400
200
0
Atm Δ14C (‰)
-6.0
-6.5
-7.0
δ13CO2 (‰)
G
H
300
240
180
CO2 (ppmv)
-42
-48
-54
EDML δ18O (‰)
I
0
5
10
15
20
25
Age (kyr)

Fig. 4

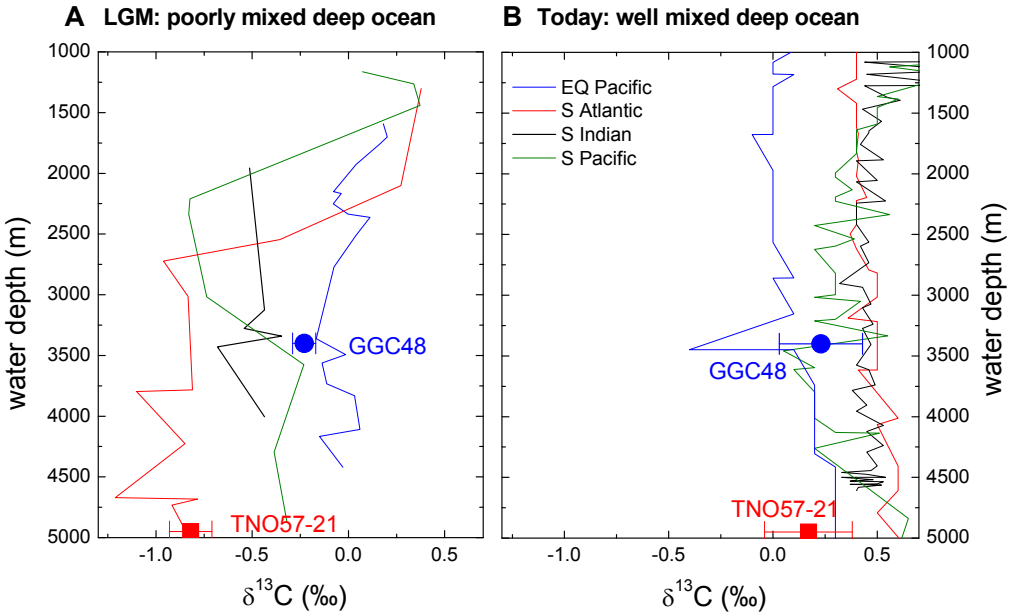
A LGM: poorly mixed deep ocean
B Today: well mixed deep ocean
water depth (m)
1000
1500
2000
2500
3000
3500
4000
4500
5000
GGC48
TNO57-21
EQ Pacific
S Atlantic
S Indian
S Pacific
-1.0
-0.5
0.0
0.5
δ13C (‰)

Fig. 5

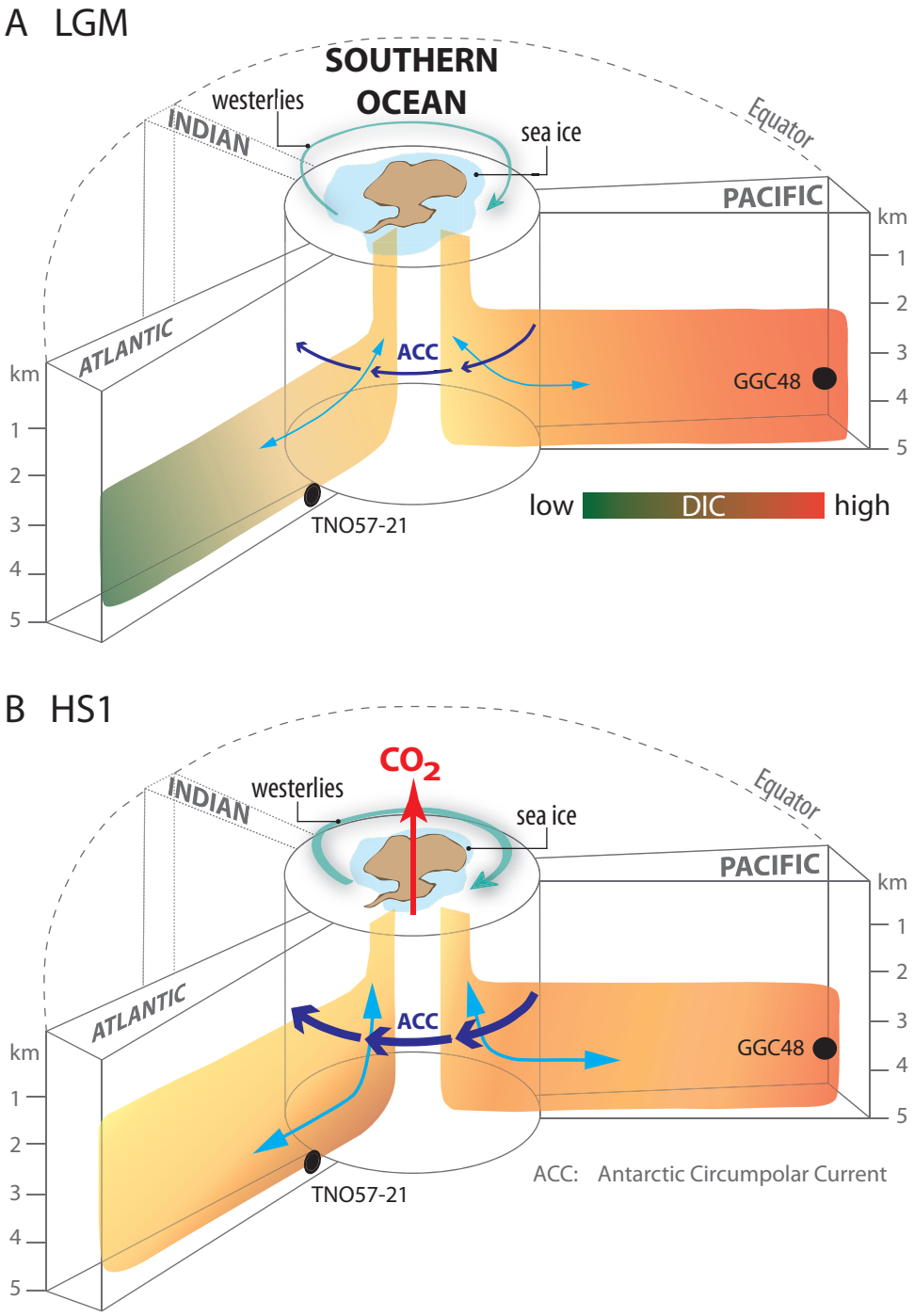
A LGM
SOUTHERN
OCEAN
westerlies
sea ice
INDIAN
Equator
PACIFIC
ATLANTIC
km
1
2
3
4
5
ACC
GGC48
TNO57-21
low
DIC
high
B HS1
CO2
INDIAN
westerlies
sea ice
Equator
PACIFIC
ATLANTIC
km
1
2
3
4
5
ACC
GGC48
TNO57-21
ACC: Antarctic Circumpolar Current

Fig. 6